Differences in the Solid-State Structures of Single-Site and Ziegler−Natta Linear Low-Density Polyethylenes As Revealed by Molecular Dynamics Simulation

Mingzong Zhang, Fanny Yuen, and Phillip Choi*

Department of Chemical & Materials Engineering, University of Alberta, Edmonton, Alberta, Canada T6G 2G6

Received March 8, 2006; Revised Manuscript Received September 15, 2006

ABSTRACT: Molecular dynamics (MD) simulations were carried out to study the solid-state structures of single-site (ss) and Ziegler−Natta (ZN) linear low-density polyethylenes (LLDPE) at a temperature slightly below their melting temperatures. The two bulk state models, used to represent the polymers, possessed the same average branch content (10 hexyl branches per 1000 backbone carbons) but with different degrees of interchain branch distribution homogeneity. Both models were first equilibrated at 463 K (i.e., 190 °C) for several nanoseconds, and the resultant structures, which were found to be representative of the corresponding liquid-state structures, were then used as the initial structures for the subsequent quenching process. The quenching temperature was 373 K (i.e., 100 °C), and the structures were then equilibrated at the same temperature for a period of about 10 ns. The structures of the two polymers formed after the low-temperature equilibrations were considerably different. In particular, the ZN-LLDPE model exhibited a higher amount of order, as quantified by a higher trans/gauche ratio, and a longer "stem length" than those of the ss-LLDPE model. The hexyl branches in the ss-LLDPE model distributed more or less evenly in its interphase and amorphous phase while the branches in the ZN-LLDPE model concentrated in the amorphous phase. The concentration of tie molecules in the ss-LLDPE model was significantly higher than that of ZN-LLDPE. We believe that the structures revealed by the MD simulations correspond to those formed in the early stages of the crystallization process since the models and simulation times used precluded us from modeling the complete crystallization process. However, it is also believed that these structures should resemble the chain conformations of the polymers in their solid state because the available thermal energy at 373 K was not sufficient for further significant conformational rearrangements. The results found are consistent with the experimental findings that ZN-LLDPE solids tend to have a higher degree of crystallinity than ss-LLDPE with similar or even lower average branch content and that ss-LLDPE solids possess a higher concentration of tie molecules. Our simulation results also indicated that with the presence of highly branched chains linear chains tended to crystallize faster than the chains with branches, and this is consistent with the experimental observation of Mirabella that thicker lamellae form before the thinner ones [*J. Polym. Sci., Part B: Polym. Phys.* **2001**, *39*, 2800].

1. Introduction

Both single-site (ss) and Ziegler−Natta (ZN) linear low-density polyethylenes (LLDPE) are commercially important materials used in a variety of products such as plastic bags, sheets, and wraps. Although the chemical structures of these two polymers are similar, their solid-state properties differ considerably. For example, ZN-LLDPE shows a higher tear resistance but a lower dart impact resistance than ss-LLDPE.[1] It is well-known that mechanical properties of LLDPE depend on the type, amount, and distribution of branches. In the literature, considerable effort has been spent on identifying the key molecular characteristics that control the observed differences in the properties of ss- and ZN-LLDPEs. In addition, it is now generally believed that the difference in the interchain branch distribution homogeneity causes the two types of polyethylenes to crystallize differently, leading to the observed differences in their mechanical properties. It is known that ZN-LLDPE tends to have a lower degree of interchain branch distribution homogeneity. In particular, most of its branches are found in the low-molecular-weight fractions of the material while only a few branches can be found on the high-molecular-weight chains. On the other hand, the interchain branch distribution of ss-LLDPE is much more homogeneous than that of ZN-LLDPE. Although extensive experimental studies of LLDPE exist, few researchers have studied the effect of the interchain branch distribution homogeneity on the structure of LLDPE at the molecular level, simply due to the limitation of the available experimental techniques. However, using techniques such as differential scanning calorimetry (DSC), nuclear magnetic resonance (NMR) spectroscopy, and temperature rising elution fraction (TREF), Mirabella has shown that there exists a two-step crystallization process for LLDPE. In particular, thicker lamellae crystallized from the longer ethylene sequences first, and later thinner lamellae formed from the shorter ethylene sequences.[2] Since computational power has increased considerably over the past two decades, it is now possible to study the detailed solid-state molecular morphologies of the two polymers using molecular simulation techniques such as molecular dynamics (MD) simulation.

Study of polyethylene crystallization using MD simulation has focused on the chain folding of single polyethylene chains in the vacuum sate, which is useful for the understanding of crystallization of polymers in dilute solutions. Using MD simulation, Kavassalis and Sundararajan found that isolated linear polyethylene chains tend to fold into lamellae via a global collapse mechanism if the torsional potential is included in the simulation. However, a two-stage collapse process was observed

* To whom correspondence should be addressed. E-mail: Phillip.choi@ualberta.ca.

10.1021/ma060516o CCC: $33.50
Published on Web 10/27/2006

without the torsional potential.[3] Later, Liao and Jin showed that modification of the torsional energy was not essential in demonstrating the local collapse mechanism.[4] Doran and Choi investigated the effect of the branch length, content, and distribution on the degree of crystallinity of model LLDPEs using MD simulation as well.[5] Most recently, Zhang et al. found that while the degree of crystallinity of LLDPE with branches shorter than 10 carbons decreases with increasing branch content, they also found that for branches with more than 10 carbons crystallinity increases with increasing branch content.[6] All of the above-mentioned MD simulations were performed on single chains in a vacuum. In this study, MD simulations of model ss- and ZN-LLDPEs using multiple chain models in the bulk state were carried out to explore the effect of interchain branch distribution homogeneity on the solid-state structures.

2. Simulation Models and Method

Two LLDPE models were built. One was used to represent ss-LLDPE while the other ZN-LLDPE. Both models contained the same type of branches—hexyl branches (i.e., branches consisted of six carbons). Each model contained 10 chains. For the ss-LLDPE model, each chain was made up with 300 CH_2 units in the backbone. Three branches were randomly attached to each chain, resulting in a branch content of 10 branches per 1000 backbone carbons. To maintain the same average branch content and to mimic its heterogeneous nature of the interchain branch distribution, among the 10 chains used in the ZN-LLDPE model, there were five chains made up with 500 CH_2 with no branches and five chains with 100 CH_2 with six branches randomly attached to each chain. The model represents the extreme case of ZN-LLDPE since the real material may contain a small amount of high-molecular-weight chains with some branches. This preliminary study does not consider the intrachain branch distribution. It is worth pointing out that there exist different views on the intrachain branch distribution of ss- and ZN-LLDPEs. Mirabella and Crist believe that for both ss- and ZN-LLDPEs the branch distribution along their corresponding backbones is random[7] while TREF results of Zhang et al. indicate that the distribution of branches in ZN-LLDPE is somewhat blocky.[8] The initial model structures of ss- and ZN-LLDPEs are shown in Figures 1a and 2a, respectively. The atoms in the structures represented by a ball indicate the locations of the branches.

Unlike the previous work reported in the literature, in which simulations were performed on single chains in a vacuum, the simulations in this work were performed in the bulk state at the experimental density; i.e., the models were subjected to three-dimensional periodic boundary conditions. To reduce the computational time, united-atom models were adopted in which all the hydrogen atoms were modeled implicitly. The initial structures of the models were constructed according to the method described by Theodorou and Suter[9] and the experimental density of polyethylene reported by Rudin et al.[10] Energy minimizations were performed to relax the initial structures, which tended to be at a high-energy state and were not suitable for MD simulation. Both the steepest-decent and conjugate gradient methods were used for the energy minimizations.[11] The energy-minimized structures were equilibrated by running canonical (i.e., NVT) MD simulations at 463 K (i.e., 190 °C), a commonly used processing temperature which is significantly higher than the experimental melting temperatures of the polymers of interest (105−115 °C), for several nanoseconds. The equilibration time was considered to be sufficient once the average center of mass of all chains displaced a distance greater than their average radius of gyration. We also calculated the end-to-end vector orientation autocorrelation function (OACF) to show that adequate equilibration was achieved at 463 K. Structures generated at the end of the high-temperature equilibration process were then used as the initial structures for the low-temperature MD equilibrations at 373 K (i.e., 100 °C) to obtain the solid-state structures. This procedure corresponds to an infinitely fast quenching process. Each system was further subjected to canonical MD equilibration at the same temperature over a period of about 10 ns to mimic the onset of the crystallization process at the liquid density.

Since our main interest here is to examine the difference in the solid-state structures between ss- and ZN-LLDPEs upon quenching, we feel justified not to determine the exact melting temperatures of the LLDPE models so long as their melting temperatures are between 373 and 463 K (see Results and Discussion). In addition, it is computationally infeasible for us to carry out such calculations, as this would require simulations of the LLDPE models over a series of temperatures.[12]

The force field we used was a modified version of the Dreiding force field.[13] Here, all the default energy expressions and the associated parameters were used except the default Lennard-Jones (LJ) parameters. Instead, we used the LJ parameters of Rychaert and Bellemans.[14] The reason for not using the default LJ parameters is that the Dreiding force field is known to have no local minima at the gauche positions. As discussed thoroughly by Sundararajan and Kavassalis,[15] use of the Dreiding force field with the default torsional barrier (2 kcal/mol) for the carbon−carbon bond rotation (the commonly accepted value is about 2.8 kcal/mol) would artificially increase the number of bonds executing the trans−gauche−nonstaggered conformational transformation, leading to a smaller lamellar dimension in the simulation of the crystallization of single chains in a vacuum. The authors found that when appropriate van der Waals energy term is combined with the default torsional barrier, the force field could yield correct total energy barrier for certain hydrocarbons. Therefore, they speculated that use of "hard" barrier for single chains in a vacuum is equivalent to introducing solvent and interchain interactions to such isolated chains. In other words, for the simulation of the bulk state with multiple chains, which is obviously the case in the present work, use of "hard" potential is not required so long as appropriate LJ parameters are used. Therefore, we used the LJ parameters of Rychaert and Bellemans rather than the default values in the Dreiding force field to alleviate its torsional problem. As can be seen in Figures 3a and 4a, there are indeed significant populations of carbon−carbon bonds at the two gauche positions at 463 K, indicating that there exist local minima and proper conformations could be obtained. In fact, we have demonstrated in our previous work that we can predict the characteristic ratio of linear polyethylene in the melt state accurately with the use of the modified Dreiding force field.[16] In particular, the characteristic ratio of polyethylene at 190 °C (463 K) was calculated to be 6.34 while the experimental value at 140 °C is 6.7.[17] Note that the temperature coefficient of polyethylene is -1.1×10^{-3}.

The Nosé canonical method and leapfrog numerical algorithm were used for the NVT MD simulations, and the integration time step was set to 1 fs.[18] All MD simulations were carried out on a Silicon Graphics workstation cluster using the commercial molecular modeling software package CERIUS^2 version 4.2 from Accerlys Inc.

3. Results and Discussion

Since crystallization is a solidification process of the melt state structure,[19] it is crucial to equilibrate the liquid-state

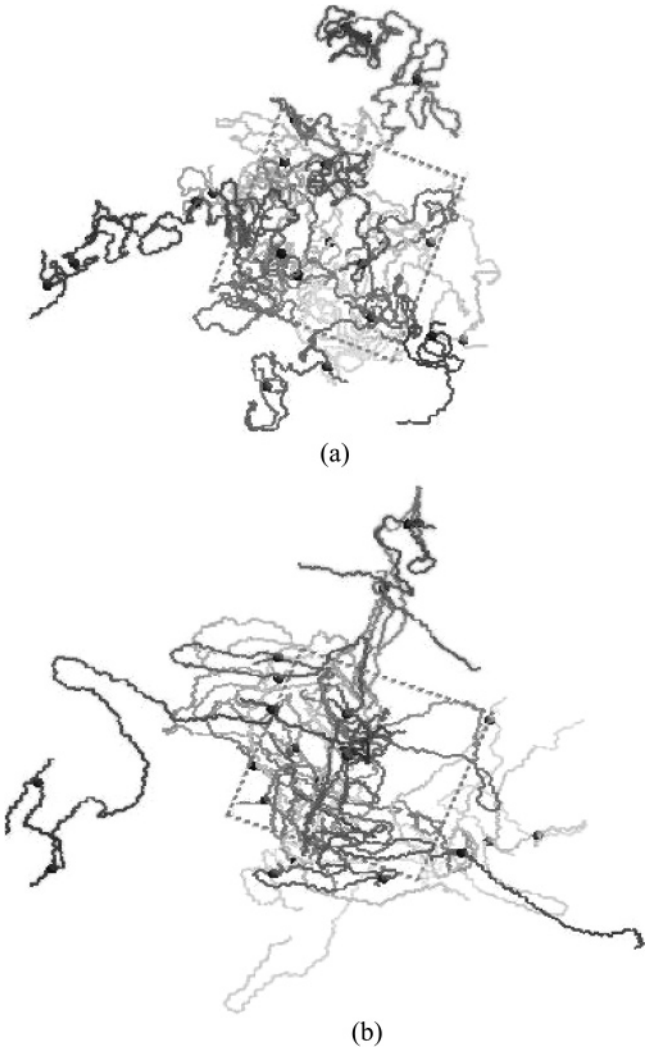

Figure 1. Structures of ss-LLDPE at 463 K: (a) 0 ns, (b) 5 ns.

models. Figures 1b and 2b show the structures after the high-temperature MD equilibration. As depicted in Figures 3a and 4a, the computed torsional angle distributions at 463 K, averaged over the last half nanosecond of the high-temperature MD simulations, show a liquidlike distribution, consistent with the rotational isomeric state model prediction.[17] As clearly shown in Figure 5, the OACFs of both LLDPE models decorrelate significantly (substantial translational motion) during the high-temperature annealing and reach a plateau (essentially no translational motion) during the MD annealing at 373 K, implying that the melting temperatures of the two models should have values between 373 and 463 K. In addition, the computed torsional angle distributions at 463 K disappear upon the MD annealing at 373 K (see Figures 3b and 4b). To show that there existed significant translational motion at 463 K and representative conformations were generated, we also calculated the root-mean-square displacements (RMSDs) of the centers of mass of all chains in both systems as well as the their average radii of gyration. The RMSD of the centers of mass of all chains in the ss-LLDPE model over the 5 ns simulation is 37.4 Å while the corresponding average radius of gyration is 23.5 Å. For the ZN-LLDPE model, the corresponding values for RMSD and average radius of gyration over 7 ns simulation are 34.6 and 30.2 Å, respectively. The results indicate that there were substantial translational motion of the chains, and the simulation times used at 463 K were long enough for equilibrating the liquid-state models as the chains had moved over a distance longer than

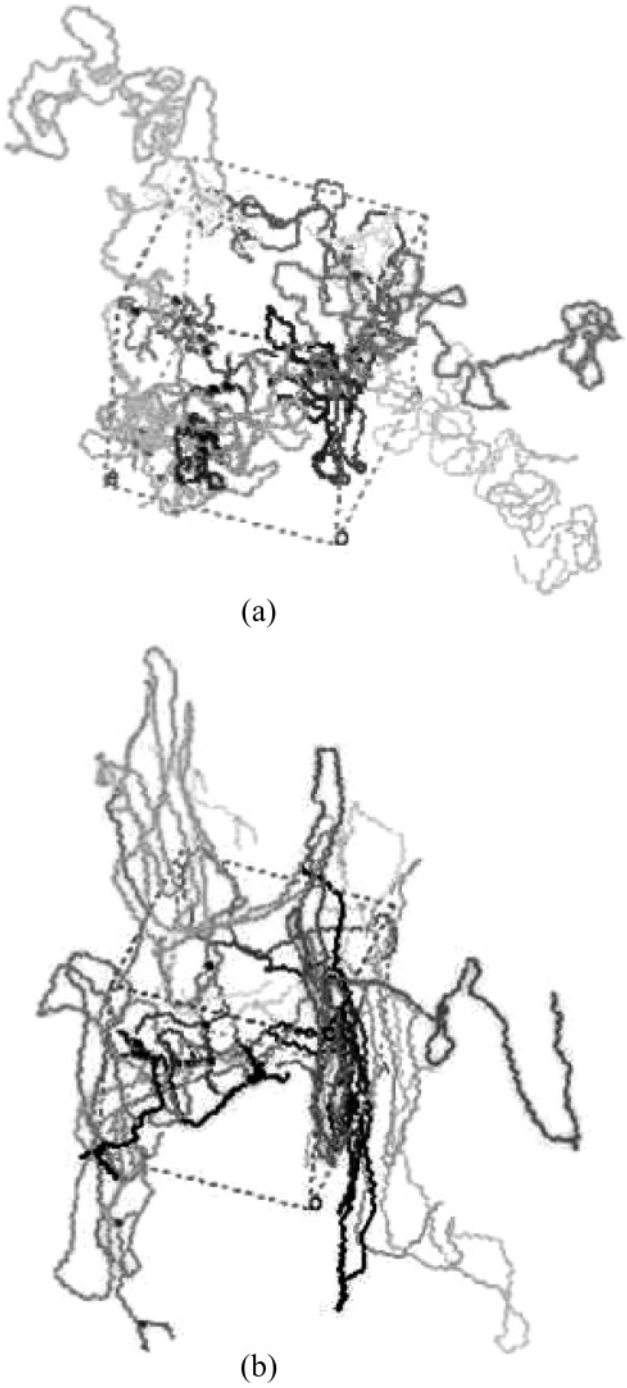

Figure 2. Structures of ZN-LLDPE at 463 K: (a) 0 ns, (b) 7.8 ns.

their corresponding average radius of gyration. It is obvious that the ZN-LLDPE model, which contained longer chains, required a longer time to equilibrate. According to the above results, we are confident that the conformations generated toward the end of the high-temperature MD simulation are representative of those in the melt state. Note that the dynamics of our systems is about 1 order of magnitude faster than that of the MD simulation results of Harmandaris et al.[20] and the experimental results of Lodge.[21] Taking their self-diffusion coefficients as the correct ones, it would take about 100 ns rather than 10 ns for the chains in our systems to move over a distance greater than their average radii of gyration. The physical origin of such discrepancy is uncertain as the force field parameters used in the present work were also used previously in our other work in which we were able to reproduce the experimental self-diffusion coefficient and heat of vaporization of *n*-heptane very

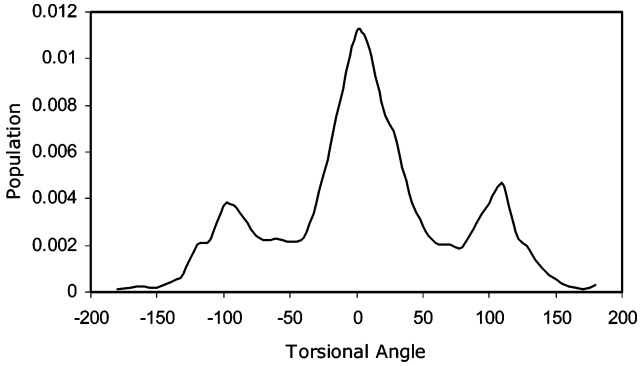

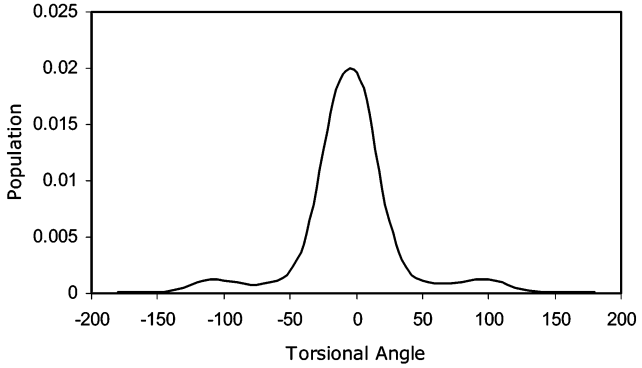

Figure 3. Torsional angle distribution of ss-LLDPE, averaged over the last half nanosecond of the respective MD simulations, at (a) 463 K and (b) 373 K.

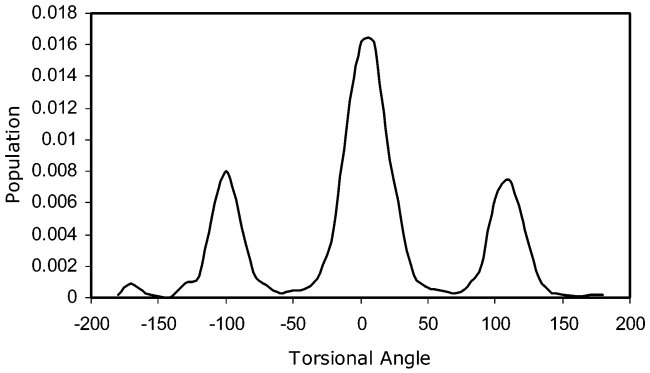

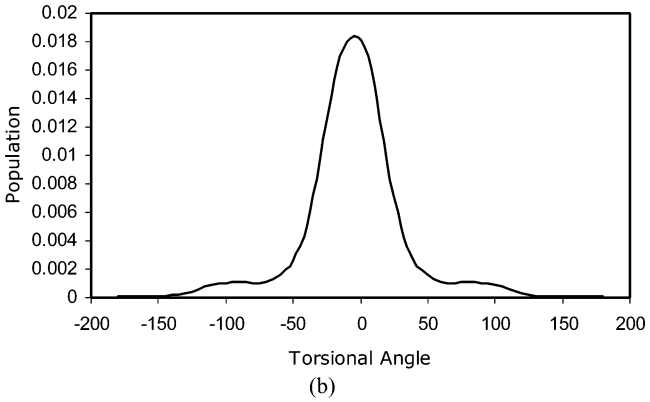

Figure 4. Torsional angle distribution of ZN-LLDPE, averaged over the last half nanosecond of the respective MD simulations, at (a) 463 K and (b) 373 K.

well.[22] Nonetheless, it is speculated that it is the intramolecular energy terms that led to the observation. There also exist

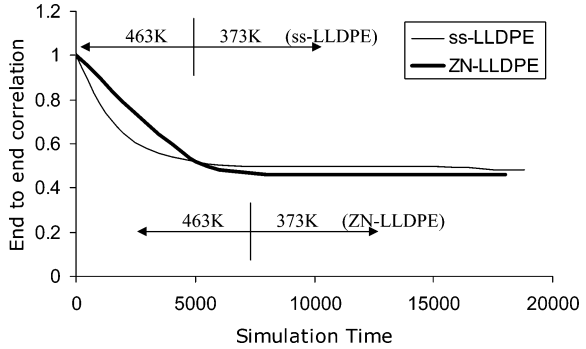

Figure 5. End-to-end vector orientation autocorrelation functions of ss- and ZN-LLDPEs.

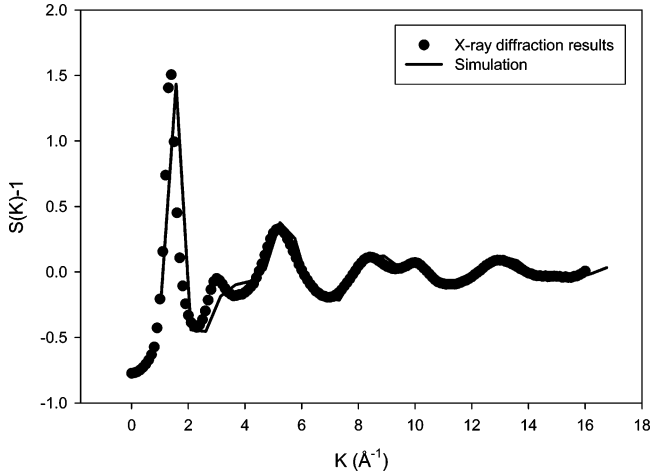

Figure 6. Simulated structure factor and X-ray diffraction patterns of linear polyethylene (X-ray diffraction data obtained from ref 24).

differences between our simulations and those of the aforementioned authors that may contribute to the differences in the results. For example, the simulation temperature we used was 463 K while the above authors used 450 K. The density we used in our simulation system at 463 K was 0.7587 g/cm^3, which was obtained from the experimental results of Rudin et al.[10] The density Harmandaris et al.[20] used was 0.8 g/cm^3. This value is much higher than the density used in this study and is much higher than the experimental density value for similar systems reported by Honnell et al.[23]

Since our primary interest is to reveal the difference in the solid-state structures of the ss-LLDPE and ZN-LLDPE models rather than to study the dynamics of the two systems, the concern here is whether the structures generated by the 463 K MD annealing are representative. Therefore, we performed a MD simulation on a polyethylene model that contained 10 linear chains, each with 300 backbone carbons, at 463 K over a simulation time of 10 ns and then compared the computed structure factor with that obtained from the X-ray diffraction experiment to check whether the modified Dreiding force field we used could yield correct liquid-state structure. The structure factor, calculated by taking the Fourier transformation of the total pair correlation function $g(r)$, can be readily obtained from the MD trajectory.

$$S(k) = 1 + \rho\left(1 - \frac{1}{N}\right)\int_0^\infty [g(r) - 1]e^{ikr}\,dr \qquad (1)$$

In eq 1, k is the wave vector, ρ is the atomic density, and N is the total number of atoms in the system. Figure 6 shows our simulation data at 463 K and the experimental data at 461 K

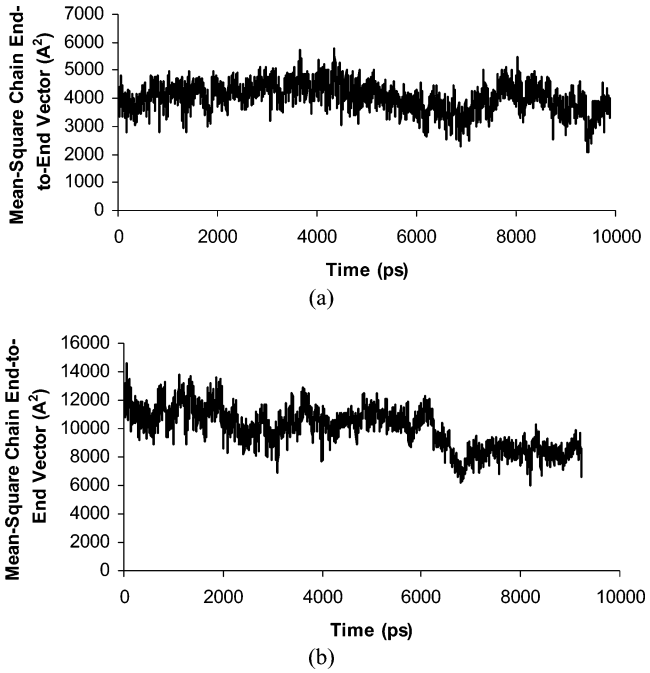

Figure 7. Time evolution of the mean-square chain end-to-end vector during the low-temperature annealing: (a) ss-LLDPE, (b) ZN-LLDPE.

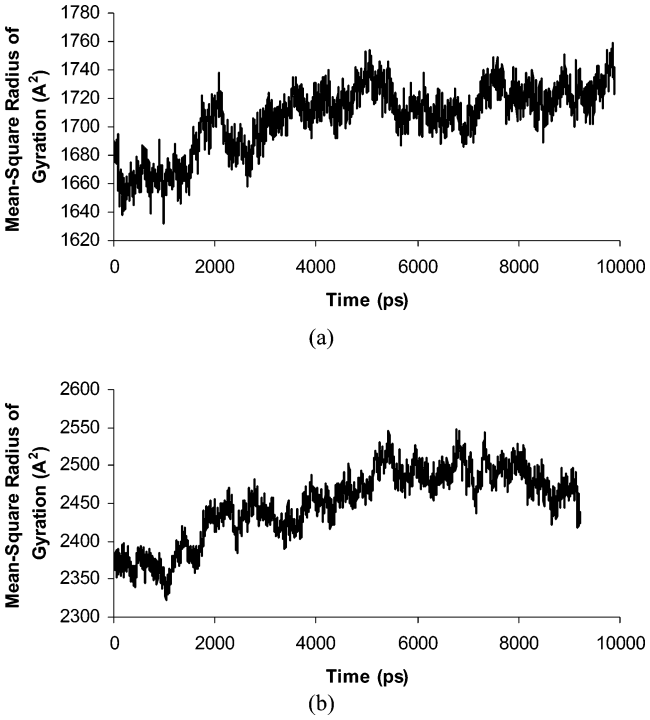

Figure 8. Time evolution of the mean-square radius of gyration during the low-temperature annealing: (a) ss-LLDPE, (b) ZN-LLDPE.

Figure 9. Structure of ss-LLDPE at 373 K (19.3 ns).

Figure 10. Structure of ZN-LLDPE at 373 K (12 ns).

measured at the Oak Ridge National Laboratory.[24] As can be seen, the agreement between our simulation and the experimental data is good except for one intramolecular peak. This suggests that our speculation on the intramolecular energy terms being the cause for the fast dynamics observed in our work may be correct and that correct interchain packing (our main interest) was obtained.

The last snapshots of ss- and ZN-LLDPE at 463 K were used as the initial structures for the subsequent MD simulations at 373 K. Comparing Figures 3a and 4a with Figures 3b and 4b, it can be seen that, at 373 K, the equilibrium torsional angle distributions no longer possess a liquidlike distribution. Figures 7 and 8 show the time evolution of the mean-square end-to-end vector and of the mean-square chain radius of gyration of the low-temperature MD equilibrations for the LLDPE models. It is clear that the mean-square radius of gyration increases gradually at the beginning of the low-temperature annealing and starts to level off later while the end-to-end vector only fluctuates at 373 K, indicating that lamellae undergo a thickening process in the early stage of the low-temperature annealing. Figures 9 and 10 depict the final structures of the ss- and ZN-LLDPE models upon the MD equilibration at 373 K. These figures, compared with Figures 1b and 2b, show that the onset of the crystallization process not only straightens chain segments but

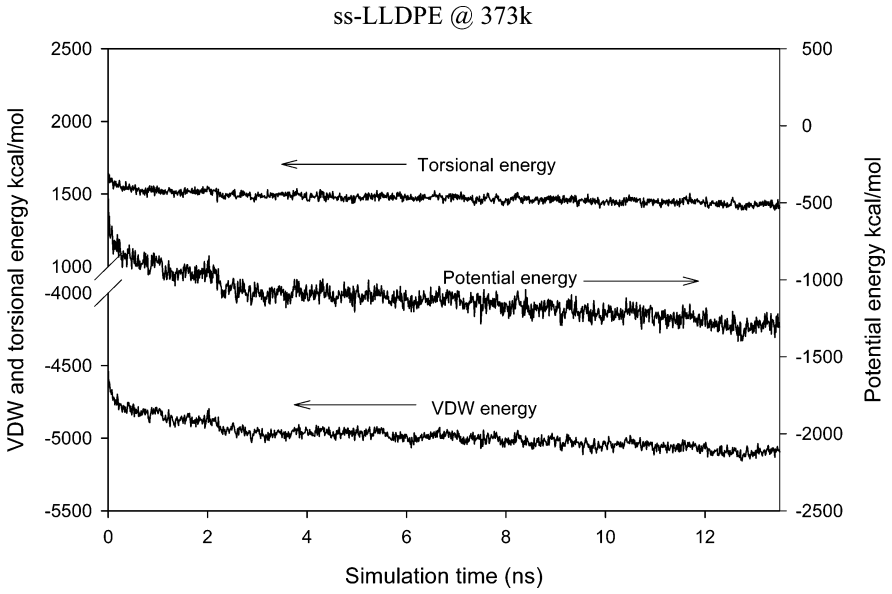

Figure 11. Energy evolution of ss-LLDPE at 373 K.

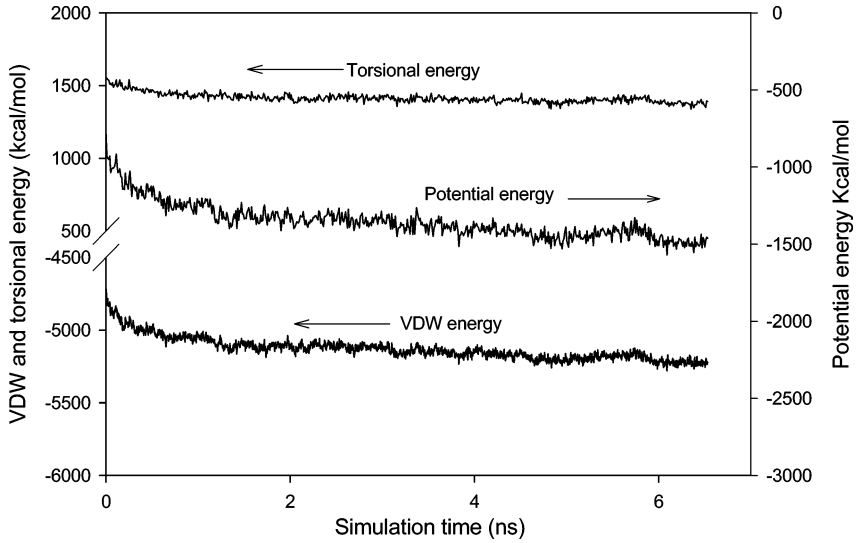

Figure 12. Energy evolution of ZN-LLDPE at 373 K.

also shows that the lateral cohesion, similar to what Qian described, occurs.[26] Such a qualitative observation manifests itself not only in the computed time evolution of the mean-square radius of gyration but also in the gradual decrease in the van der Waals energy and torsional energy in the energy evolution curves shown in Figures 11 and 12. Here, it is worth noting that the decrease in the potential energy during the low-temperature simulation is mainly attributed to the decrease in the van der Waals energy. And it is expected that the above-mentioned solidification process would lead to an increase in density of the material if the simulations could be performed over a much longer time and the volume of the simulation box was allowed to change. Therefore, it is not expected that the energy of the models would decrease indefinitely.

Similar to our previous work,[5] the trans/gauche (t/g) ratio is used to quantify the amount of order present in the models. Here, the trans state is defined as the conformational state of a bond with torsion angles around $0 \pm 10°$ and the gauche states, including both gauche plus and gauche minus, of a bond with torsion angles around $\pm 100 \pm 10°$. The shifts of the gauche torsion angles are a result of the use of the united atom models. Figure 13 shows the t/g ratio as a function of simulation time

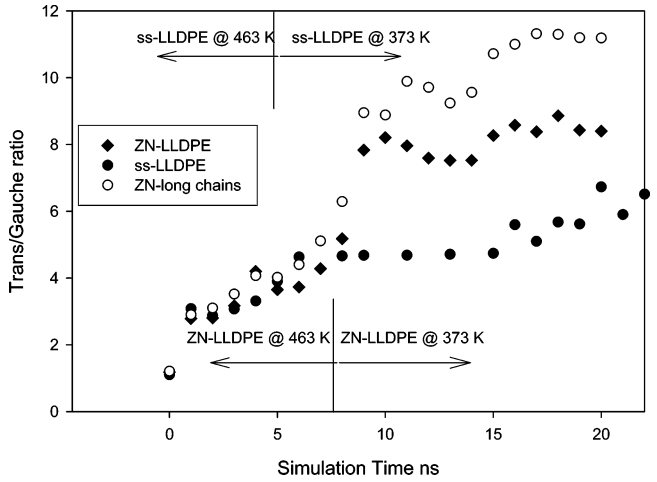

Figure 13. Trans/gauche ratios of ss- and ZN-LLDPEs at 463 and 373 K.

at 463 and 373 K for the ss- and ZN-LLDPE models. The initial structures of both models had a t/g ratio of about one, indicating that the initial torsion angle assignments were purely random,

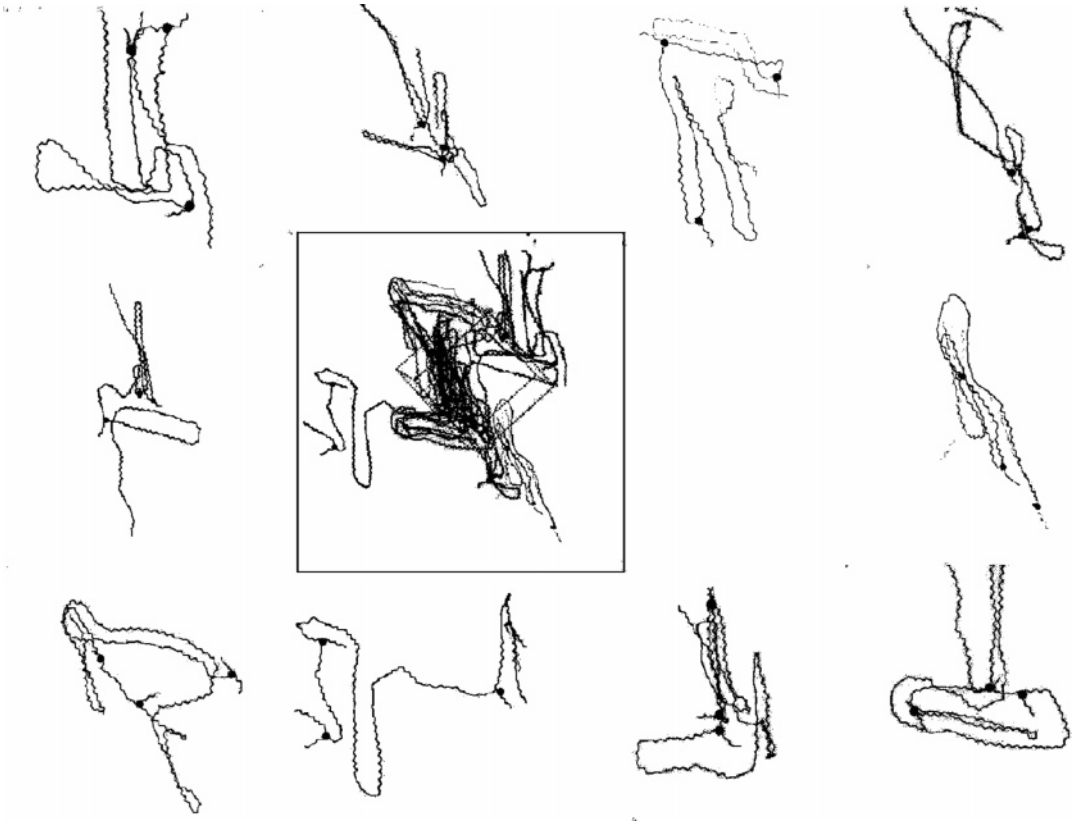

Figure 14. Individual chain conformations of ss-LLDPE at 373 K.

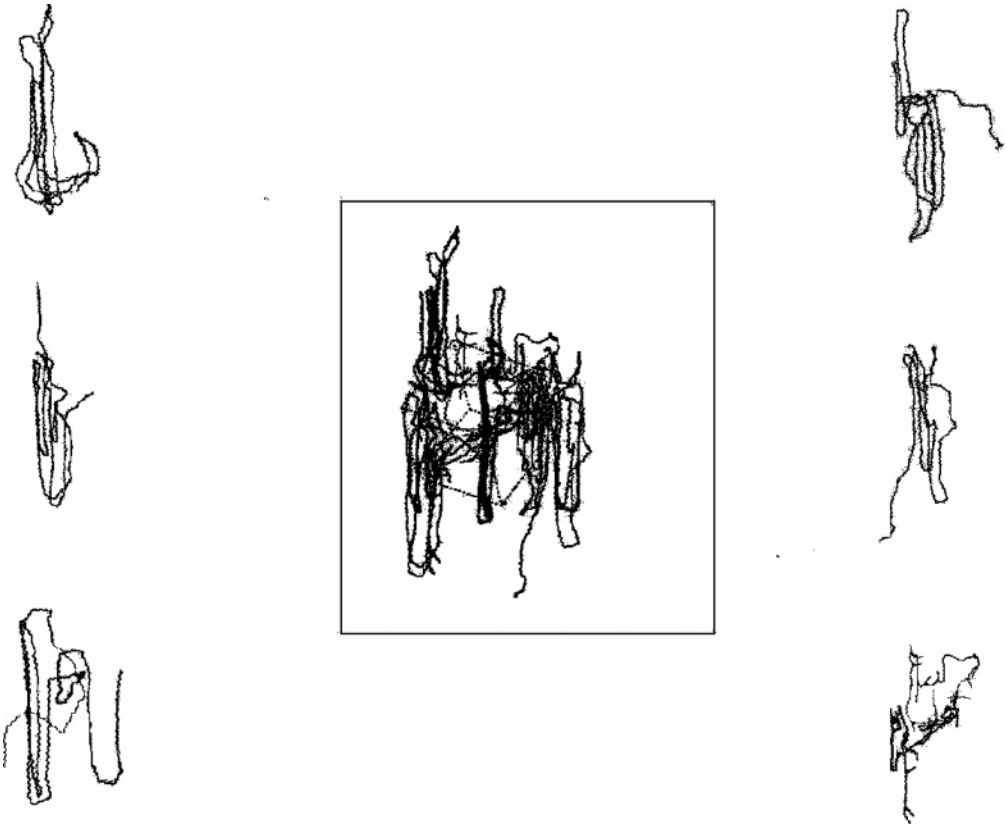

Figure 15. Individual chain conformations of ZN-LLDPE at 373 K.

and there existed no preference for the chains to be in the trans or gauche state. At 463 K, in the first 1 ns, the t/g ratio for both models increases rapidly with simulation time. After such an initial period, the t/g ratio's rate of increase became moderate. However, after the models were quenched to 373 K, the t/g ratio of ZN-LLDPE exhibited a much higher quantum jump than ss-LLDPE. Moreover, the majority of the increase in the t/g ratio for ZN-LLDPE is due to the long 500 carbon chains.

This implies that in a melt that contains both branched and linear chains the linear chains will tend to crystallize first. Extrapolating this result, chains with fewer branches will crystallize before chains with more branches. This is consistent with the result of Mirabella,[2] who concluded that thicker crystallites (chains with no or fewer branches) form before thinner crystallites (chains with more branches). Although the Dreiding force field cannot accurately capture the dynamics of LLDPE in the melt state, it has been used successfully, by many other researchers, to identify qualitative trends as a function of molecular structure. Here, the rationale for presenting Figure 13 and for making the above conclusion is attributed to our belief that the force field could capture the relative "crystallization rate" qualitatively. Figure 13 also shows that, compared with the ss-LLDPE model, the ZN-LLDPE model has higher t/g ratios over the simulation time at 373 K. The result suggests that ZN-LLDPE solids have higher degree of crystallinity than ss-LLDPE with comparable average branch content under similar crystallization conditions. The final snapshots of the simulations at 373 K show that the lamellar thicknesses of the two LLDPE models are quite different (see Figures 9 and 10). In particular, the lamellae formed in the ss-LLDPE model consisted of an average of 24 carbons while the ZN-LLDPE model 34 carbons. Since, in the ss-LLDPE model, branches are randomly distributed along the backbones and are excluded from the crystallites, there is a significant reduction in the crystallizability of the ethylene sequences. On the other hand, since all branches in the ZN-LLDPE model are on the low-molecular-weight chains and these chains tend not to crystallize, only the longer chains of the system crystallize. Kuwabara et al.[26] also observed the difference in the degree of crystallinity between these two LLDPEs. They showed that for butyl branched ss-LLDPE and ZN-LLDPE with similar average branch content the melting temperature of ZN-LLDPE is about 10 deg higher than that of ss-LLDPE, suggesting that ZN-LLDPE possesses thicker lamellae. Their transmission electron microscopy (TEM) results also support these findings.[26] More recently, Gelfer and Winter showed that even for ss-LLDPE that has lower average branch content than ZN-LLDPE, the melting temperature of ss-LLDPE is still lower than that of ZN-LLDPE, which means that besides the average branch content the interchain branch distribution homogeneity also plays an important role in the crystallization of LLDPEs.[27] It is believed that the higher degree of crystallinity of ZN-LLDPE contributes to its higher tear resistance compared to ss-LLDPE. This is because lamellae are likely to act as obstacles for crack propagation.[28,29]

Our simulation results also show that the molecular morphologies of these two polymers are quite different. The single-chain conformations of ss- and ZN-LLDPEs shown in Figures 9 and 10 are presented in Figures 14 and 15, respectively, to illustrate the major difference between the chain-folding pattern of these two LLDPEs. It should be noted that, in Figure 15, the five short chains used in the ZN-LLDPE model are shown together at the lower right-hand corner while the other chains shown are the five linear chains without branches. Figure 16a,b shows the corresponding schematics of their molecular morphologies. For ss-LLDPE, it seems that the interchain branch distribution homogeneity causes the chains to go through different crystalline regions rather than reentry into the same lamella (see Figures 14 and 16a). As a result, the branches tend to distribute more or less evenly in the hairpin structure and in the amorphous phase. If we regard the branches located in the hairpin structure as in the interphase and the others as the amorphous phase, then, in the present work, about 40% of the branches are located in the interphase and the remaining 60% in the amorphous phase. The results of the ZN-LLDPE model show that chains without branches are more likely to reenter into the same lamella rather than into a different one (see Figures 15 and 16b) in the presence of highly branched chains. The short chains with branches are excluded to only the amorphous phase. This is because the average ethylene sequence length between branches in the short chains used in the ZN-LLDPE model is about 16 carbons, which is not long enough to form lamellae. Compared with ZN-LLDPE, chains of ss-LLDPE are more likely to enter into different lamellae in the material, which results in a higher concentration of tie molecules. The tie molecules in the amorphous phase exist in a variety of forms. Some are entangled while others form local orders in the amorphous phase, which can be seen from the ss-LLDPE conformation in Figure 14. Here, the tie chains are defined as the chains that link or transverse more than one "lamella" region. This observation is consistent with the experimental findings. For ss-LLDPE with short butyl branches, the tie molecule fraction increases with increasing branch content, and the optimum condition for tie molecules formation in LLDPE is when the spacing between branches is close to the thickness of lamellae.[30] One of the reasons we set the branch content of

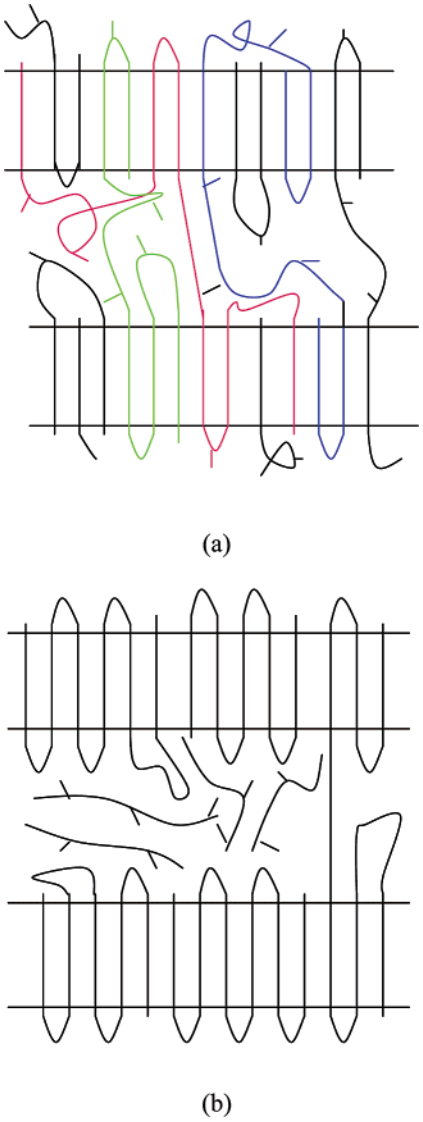

Figure 16. Schematics of solid-state molecular morphologies of (a) ss-LLDPE and (b) ZN-LLDPE.

our LLDPE models to 10 hexyl branches per 1000 backbone carbons is because it has been found that at a branch content of 10 butyl branches per 1000 backbone carbons the tie molecule concentration reaches a maximum.[1] Obviously, in real ZN-LLDPE, there are branches present in the high-molecular-weight chains, which will yield a certain amount of tie molecules. Therefore, our simulation results suggest that the tie molecules concentration can be manipulated by incorporating a controlled amount of branches into the higher molecular weight chains at proper locations along the backbone and that the intrachain branch distribution is an important parameter to be controlled. Since tie molecules are able to transfer stress effectively from one lamella to the next when strained, it is believed that the tie molecule concentration plays an important role in determining certain mechanical properties of polyethylene. In fact, Janimak and Stevens showed that the dart impact strength of ss-LLDPE correlates well with its branch content and therefore the tie molecules concentration.[30] Our simulation results for the tie molecules concentration is supported by the fact that ss-LLDPE has a higher impact strength than that of ZN-LLDPE.[1]

In general, the higher the molecular weight of a linear polyethylene, the higher the concentration of tie molecules. However, in the current simulations, it was observed that the chains used in the ss-LLDPE model (each chain contained 300 carbons) tended to form more tie molecules than ZN-LLDPE (five chains contained 500 carbons). This is not in contradiction to the observation found in the linear polyethylene. Rather, our results indicate that the presence of highly branched chains in a polyethylene sample would suppress the formation of tie molecules of the high-molecular-weight chains.

4. Conclusion

In this work, we performed MD simulation of model ss- and ZN-LLDPEs with the same average branch content under bulk conditions but with different degrees of interchain branch distribution homogeneity. The simulation results show that for ss-LLDPE the branches were distributed in the interphase and amorphous phase fairly evenly. However, the branches are more likely to be located in the amorphous phase for ZN-LLDPE. Because of the branch distribution difference, the chains in the ss-LLDPE model are more inclined to extend to several lamellae while the linear chains used in the ZN-LLDPE model more easily reenter into the same lamella. This causes ss-LLDPE to have a higher concentration of tie molecules than ZN-LLDPE. The simulation results also show that, compared with ss-LLDPE, ZN-LLDPE has a higher degree of crystallinity and a longer average crystalline stem length.

Acknowledgment. We thank NOVA Chemicals Corporation and the Natural Science Research Council of Canada for supporting this work financially. We also thank Chunli Li for the preparation of the figures. This research has been enabled by the use of WestGrid computing resources, which are funded in part by the Canada Foundation for Innovation, Alberta Innovation and Science, BC Advanced Education, and the participating research institutions. WestGrid equipment is provided by IBM, Hewlett-Packard, and SGI.

References and Notes

(1) Guichon, O.; Séguéla, R.; David, L.; Vigier, G. *J. Polym. Sci., Part B: Polym. Phys.* **2003**, *41*, 327.
(2) Mirabella, F. M. *J. Polym. Sci., Part B: Polym. Phys.* **2001**, *39*, 2800.
(3) Kavassalis, T. A.; Sundararajan, P. R. *Macromolecules* **1993**, *26*, 4144.
(4) Liao, Q.; Jin, X. G. *J. Chem. Phys.* **1999**, *110*, 8835.
(5) Doran, M.; Choi, P. *J. Chem. Phys.* **2001**, *115*, 2827.
(6) Zhang, X. B.; Li, Z. S.; Yang, H.; Sun, C. C. *Macromolecules* **2004**, *37*, 7393.
(7) Mirabella, F. M.; Crist, B. *J. Polym. Sci., Part B: Polym. Phys.* **2004**, *42*, 3416.
(8) Zhang, M.; Lynch, D. T.; Wanke, S. E. *Polymer* **2002**, *43*, 1497.
(9) Theodoru, D. N.; Suter, U. W. *Macromolecules* **1985**, *18*, 1467.
(10) Rudin, A.; Chee, K. K.; Shaw, J. H. *J. Polym. Sci., Part C: Polym. Symp.* **1970**, *30*, 415.
(11) Spyriouni, T.; Vergelati, C. *Macromolecules* **2001**, *34*, 5306.
(12) Xu, G.; Mattice, W. L. *J. Chem. Phys.* **2002**, *117*, 3440.
(13) Mayo, S. L.; Olafson, B. D.; Goddard, W. A., III. *J. Chem. Phys.* **1990**, *94*, 8897.
(14) Rychaert, J. P.; Bellemans, A. *Chem. Phys. Lett.* **1975**, *30*, 123.
(15) Sundararajan, P. R.; Kavassalis, T. A. *J. Chem. Soc., Faraday Trans.* **1995**, *91*, 2541.
(16) Zhao, L.; Choi, P. *Polymer* **2004**, *45*, 1349.
(17) Rehahn, M.; Mattice, W. L.; Suter, U. W. *Rotational Isomeric State Models in Macromolecular Systems*; Springer-Verlag: New York, 1997.
(18) Allen, M. P.; Tildesley, D. J. *Computer Simulation of Liquids;* Oxford University Press: Oxford, 1987.
(19) Fischer, E. W. *Pure Appl. Chem.* **1978**, *50*, 1319.
(20) Harmandaris, V. A.; Mavrantzas, V. G.; Theodorou, D. N.; Kroger, M.; Ramirez, J.; Ottinger, H. C.; Vlassopoulos, D. *Macromolecules* **2003**, *36*, 1376.
(21) Lodge, T. P. *Phys. Rev. Lett.* **1999**, *93*, 3218.
(22) Zhao, L.; Choi, P. *J. Chem. Phys.* **2004**, *120*, 1935.
(23) Honnell, K. G.; McCoy, J. D.; Curro, J. G.; Schweizer, K. S.; Narten, A. H.; Habenschuss, A. *J. Chem. Phys.* **1991**, *94*, 4659.
(24) Habenschuss, A. Private communication, Oak Ridge National Laboratory.
(25) Qian, R. Y. *J. Macromol. Sci., Phys.* **2001**, *40*, 1131.
(26) Kuwabara, K.; Kaji, H.; Horii, F.; Bassett, D. C.; Olley, R. H. *Macromolecules* **1997**, *30*, 7516.
(27) Gelfer, Y.; Winter, H. *Macromolecules* **1999**, *32*, 8974.
(28) Kim, Y. M.; Park, J. K. *J. Appl. Polym. Sci.* **1996**, *61*, 2315.
(29) Kim, Y. M.; Kim, C. H.; Park, J. K.; Lee C. W.; Min, T. I. *J. Appl. Polym. Sci.* **1997**, *63*, 289.
(30) Janimak, J. J.; Stevens, C. G. *J. Mater. Sci.* **2001**, *36*, 1879.

MA060516O